Entanglement distribution in Bhabha scattering with an entangled spectator particle

Massimo Blasone,[*] Gaetano Lambiase,[†] and Bruno Micciola[‡]

Dipartimento di Fisica, Università di Salerno, Via Giovanni Paolo II, 132 I-84084 Fisciano (SA), Italy and INFN, Sezione di Napoli, Gruppo collegato di Salerno, Italy

(Received 31 January 2024; accepted 22 April 2024; published 16 May 2024)

We analyze how entanglement is generated and distributed in a Bhabha scattering process ($e^-e^+ \to e^-e^+$) at tree level. In our setup an electron A scatters with a positron B, which is initially entangled with another electron C (spectator), that does not participate directly to the process. We find that the QED scattering generates and distributes entanglement in a nontrivial way among the three particles; the correlations in the output channels AB, AC, and BC are studied in detail as functions of the scattering parameters and of the initial entanglement weight. Although derived in a specific case, our results exhibit some general features of other similar QED scattering processes, for which the extension of the present analysis is straightforward.

DOI: 10.1103/PhysRevD.109.096022

I. INTRODUCTION

The role of entanglement in high-energy physics has recently become a very active research area [1–63]. Much attention has been devoted to the study of quantum correlations in neutrino oscillations [7–33], since neutrinos are regarded as possible alternative carriers of quantum information with respect to photons. Various aspects of entanglement in scattering processes have been investigated in the context of different fundamental interactions [34–63]. In Refs. [40–42] entanglement and other types of quantum correlations have been studied in top-antitop quark pairs, using the experimental data from proton-proton and proton-antiproton collision at the LHC.

In Refs. [47,48] maximal entanglement generated at the fundamental level in QED by studying correlations between helicity states at tree-level for various scattering processes is analyzed. In particular, the authors describe the mechanisms that generate maximal entanglement and its relation with the scattering amplitudes in the high-energy regime. An extension of this work is given in Ref. [50], where the entanglement generation was analyzed at all energies for pure and mixed final states for arbitrary initial mixtures of helicity states. It was shown that maximal entanglement can originate in all situations where one dominating channel leads to balanced superpositions of helicity states. It was also argued that loop corrections do not significantly alter the results obtained at tree level.

An interesting extension of these studies is given in Refs. [51,52]. In Ref. [51] it is considered a QED scattering of two particles A and B, in which B is initially entangled with a third particle C that does not participate directly in the process. The authors investigate the effects of the scattering both on the particle C and in the bipartite channels. In Ref. [52] the model is extended by considering a general three-partite entangled state in input and applied to the case of QED inelastic tree-level process $e^-e^+ \to \mu^-\mu^+$. Further extensions of these works are given in Refs. [53,54].

In this work, starting from the same framework used in Ref. [51], we study in detail the case of Bhabha scattering, describing how entanglement is generated and distributed in the three bipartite subsystems AB, AC, and BC after the scattering as represented in Fig. 1. This process depends on the value of the initial entanglement weight η and of the scattering parameters θ (scattering angle) and μ (the ratio between $\vec{p}$ the incoming momentum of e^- and e^+ in the center of mass (COM) reference frame and m the particles mass). For incoming momenta of the order of the mass, the entanglement has a nontrivial distribution in the three output channels. On the other hand, in the relativistic regime, the interaction behaves like a perfect quantum gate; for specific values of parameters, the entanglement transfers completely from the BC bipartition (where was initially present) to the AC bipartition.

The paper is organized as follows. In Sec. II we set up the problem and analyze the density matrix structure for the C subsystem, relative to the spectator particle, before and after the scattering. In Sec. III we study the entanglement generation in the scattering between A and B, taking B as a superposition of helicity states. The study of such a reference state is useful for the analysis carried out in Sec. IV, where we consider the entanglement generation and distribution in the presence of a spectator particle C. Section V is devoted to conclusions and outlook.

[*]blasone@sa.infn.it
[†]lambiase@sa.infn.it
[‡]bmicciola@unisa.it

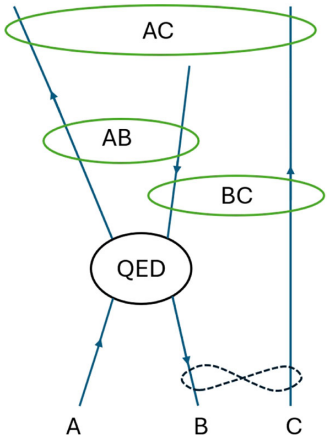

FIG. 1. Schematic representation of the process considered in this work. Particles A and B scatter through a QED process at tree level. Particle C (spectator) does not participate to the scattering and is initially entangled to particle B. The ellipses AB, AC, and BC represent the bipartitions for which we calculate the entanglement.

II. ENTANGLEMENT IN QED SCATTERING WITH SPECTATOR PARTICLES

In this section we briefly recall the setup used in Ref. [51], in which it is considered a general QED scattering process at tree level involving two particles ($AB \to AB$), where B, before the interaction, is entangled in spin with a third particle C that does not participate to the process, as schematically shown in Fig. 1. For simplicity, we perform our calculations in the COM reference frame for particles A and B and assume that the spectator momentum $\mathbf{q}$ is aligned in the same direction of the incoming momenta of A and B.

The internal product of fermion states is defined as

$$\langle k, a|p, b\rangle = 2E_{\mathbf{k}}(2\pi)^3\delta^{(3)}(\mathbf{k}-\mathbf{p})\delta_{a,b}, \tag{1}$$

where k and p are the 4-momenta and a and b are the spin indices.

The initial state is taken to be

$$|i\rangle = |p_1, a\rangle_A \otimes (\cos\eta|p_2, \uparrow\rangle_B \otimes |q, \uparrow\rangle_C + e^{i\beta}\sin\eta|p_2, \downarrow\rangle_B \otimes |q, \downarrow\rangle_C), \tag{2}$$

whose final state, is given by

$$|f\rangle = |i\rangle + i\sum_{r,s}\int \frac{d^3\mathbf{p_3}d^3\mathbf{p_4}}{(2\pi)^6 2E_{\mathbf{p_3}}2E_{\mathbf{p_4}}}\delta^{(4)}(p_1+p_2-p_3-p_4)[\cos\eta\mathcal{M}(a,\uparrow;r,s)|p_3,r\rangle_A \otimes |p_4,s\rangle_B \otimes |q,\uparrow\rangle_C$$
$$+ e^{i\beta}\sin\eta\mathcal{M}(a,\downarrow;r,s)|p_3,r\rangle_A \otimes |p_4,s\rangle_B \otimes |q,\downarrow\rangle_C]. \tag{3}$$

The partial trace operation is given by

$$\mathrm{Tr}_X[\rho] = \sum_\sigma \int \frac{d^3\mathbf{k}}{(2\pi)^3 2E_{\mathbf{k}}}(\mathbb{I}_r \otimes {}_X\langle k,\sigma|)\rho(\mathbb{I}_r \otimes |k,\sigma\rangle_X), \tag{4}$$

where $\mathbb{I}_r$ denotes the identity operation in the remaining subspaces, k and σ are the 4-momentum and spin indices as before and X is the generic space with respect to which we calculate the trace.

In Eq. (3), $\mathcal{M}(a,\uparrow;r,s)$ represents the scattering amplitude $\mathcal{M}(p_1,a,p_2,\uparrow;p_3,r,p_4,s)$ and the same for $\mathcal{M}(a,\downarrow;r,s)$, where we have omitted initial and final momenta for brevity. We can describe the final states in terms of the density matrix as

$$\rho^f_{ABC} = \frac{1}{\mathcal{N}}|f\rangle\langle f|, \tag{5}$$

where $\mathcal{N}$ is the normalization constant. Using Eq. (4) and applying the following relations:

$$2\pi\delta^{(0)}(E_i - E_f) = \int_{-T/2}^{T/2} e^{i(E_i-E_f)t}dt, \tag{6}$$

$$(2\pi)^3\delta^{(3)}(\mathbf{k}-\mathbf{p}) = V\delta_{\mathbf{k},\mathbf{p}}, \tag{7}$$

which imply that $(2\pi)\delta^{(0)}(0) = T$ and $(2\pi)^3\delta^{(3)}(0) = V$, we can easily compute the normalization constant $\mathcal{N}$,

$$\mathcal{N} = Tr_A[Tr_B[Tr_C[|f\rangle\ \langle f|]]] = 2E_{p_1}2E_{p_2}2E_qV^3 + 2E_qT^2V^2\Lambda, \tag{8}$$

where

$$\Lambda = \int \frac{d^3\mathbf{p_3}}{(2\pi)^3 2E_{\mathbf{p}_3} 2E_{\mathbf{p_3}-\mathbf{p_1}-\mathbf{p_2}}} \sum_{r,s} (\cos^2\eta |\mathcal{M}(a,\uparrow;r,s)|^2 + \sin^2\eta |\mathcal{M}(a,\downarrow;r,s)|^2)|_{\mathbf{p_4}=\mathbf{p_3}-\mathbf{p_1}-\mathbf{p_2}}. \tag{9}$$

A. Effects of scattering on spectator particle

We now investigate the effects of the scattering over the spectator particle C. To this aim, we consider the reduced density matrix,

$$\rho_C \equiv \mathrm{Tr}_A[\mathrm{Tr}_B[\rho_{ABC}]], \tag{10}$$

relative to the C subsystem, both for the initial and the final states.

By using Eq. (4) to calculate the reduced density matrix for C from the initial state Eq. (2), we get

$$\rho_C^i = 2E_{\mathbf{p_1}} 2E_{\mathbf{p_2}} (\cos^2\eta |\uparrow\rangle_{CC}\langle\uparrow| + \sin^2\eta |\downarrow\rangle_{CC}\langle\downarrow|) \otimes |q\rangle_{CC}\langle q|. \tag{11}$$

From now on, as the entanglement is consider over the spin degrees of freedom, we omit the factorized part $|q\rangle_{CC}\langle q|$ of the spectator momentum subspace. The initial C-density matrix can be express in matrix form as

$$\rho_C^i = \begin{pmatrix} \cos^2\eta & 0 \\ 0 & \sin^2\eta \end{pmatrix}. \tag{12}$$

The reduced density matrix of the final state for C reads,

$$\begin{aligned}
\rho_C^f =& \frac{1}{\mathcal{N}} \sum_{\sigma\sigma'} \int \frac{d^3\mathbf{k} d^3\mathbf{k}'}{(2\pi)^6 2E_{\mathbf{k}} 2E_{\mathbf{k}'}} (\mathbb{1}_r \otimes {}_B\langle k'\sigma'|_A \langle k\sigma|)|f\rangle\langle f|(|k\sigma\rangle_A |k'\sigma'\rangle_B \otimes \mathbb{1}_r) \\
=& \frac{1}{\mathcal{N}} \Bigg\{ 2E_{\mathbf{p_1}} 2E_{\mathbf{p_2}} V^2 (\cos^2\eta |\uparrow\rangle_{CC}\langle\uparrow| + \sin^2\eta |\downarrow\rangle_{CC}\langle\downarrow|) \\
&+ T^2 V \int \frac{d^3\mathbf{p_3}}{(2\pi)^3 2E_{\mathbf{p}_3} 2E_{\mathbf{p_1}+\mathbf{p_2}-\mathbf{p_3}}} \Bigg[\sum_{rs} (\cos^2\eta |\mathcal{M}(a,\uparrow;r,s)|^2 |\uparrow\rangle_{CC}\langle\uparrow| + e^{-i\beta}\cos\eta\sin\eta \mathcal{M}(a,\uparrow;r,s)\mathcal{M}^\dagger(a,\downarrow;r,s)|\uparrow\rangle_{CC}\langle\downarrow| \\
&+ e^{i\beta}\cos\eta\sin\eta \mathcal{M}(a,\downarrow;r,s)\mathcal{M}^\dagger(a,\uparrow;r,s)|\downarrow\rangle_{CC}\langle\uparrow| + \sin^2\eta |\mathcal{M}(a,\downarrow;r,s)|^2 |\downarrow\rangle_{CC}\langle\downarrow|) \Bigg] \Bigg\} \otimes |q\rangle_{CC}\langle q|.
\end{aligned} \tag{13}$$

This, in matrix form as before, looks like

$$\rho_C^f = \frac{1}{\mathcal{N}} \begin{pmatrix} (2E_{\mathbf{p_1}} 2E_{\mathbf{p_2}} V^2 + \int_{\mathbf{p}_3} \sum_{rs} |\mathcal{M}(a,\uparrow;r,s)|^2)\cos^2\eta & e^{-i\beta}\cos\eta\sin\eta \int_{\mathbf{p}_3} \sum_{rs} \mathcal{M}(a,\uparrow;r,s)\mathcal{M}^\dagger(a,\downarrow;r,s) \\ e^{i\beta}\cos\eta\sin\eta \int_{\mathbf{p}_3} \sum_{rs} \mathcal{M}(a,\downarrow;r,s)\mathcal{M}^\dagger(a,\uparrow;r,s) & (2E_{\mathbf{p_1}} 2E_{\mathbf{p_2}} V^2 + \int_{\mathbf{p}_3} \sum_{rs} |\mathcal{M}(a,\downarrow;r,s)|^2)\sin^2\eta \end{pmatrix}, \tag{14}$$

where we have defined the shorthand notation, $\int_{\mathbf{p}_3} \equiv T^2 V \int \frac{d^3\mathbf{p_3}}{(2\pi)^3 2E_{\mathbf{p_3}} 2E_{\mathbf{p_1}+\mathbf{p_2}-\mathbf{p_3}}}$.

Now, fixing the incoming momentum, we can study the system in terms of the helicity states. Using the spinors reported in Appendix A and considering the specific case of Bhabha scattering, we calculate the scattering amplitude and the elements of the matrix ρ_C^f, with an arbitrary initial polarized state for e^+ and e^-.

The off-diagonal terms in Eq. (14) vanish identically[1]; the expression $\sum_{rs} \mathcal{M}(a,\uparrow;r,s)\mathcal{M}^\dagger(a,\downarrow;r,s)$ is an odd function of the scattering angle θ.

[1]In Ref. [54], in the context of Compton scattering, by resorting to unitarity and to the optical theorem, a similar conclusion is obtained.

The diagonal terms turn out to be the same of those of ρ_C^i. Thus, we have

$$\rho_C^i = \rho_C^f = \begin{pmatrix} \cos^2\eta & 0 \\ 0 & \sin^2\eta \end{pmatrix}. \tag{15}$$

The same conclusion holds for the unpolarized case and for other QED scattering processes. This ensures that if C is out of the light cone of the scattering event, no superluminal communication can occur; as a consequence, the C observer cannot get any information about the scattering process, whatever the observable he/she measures. This result is in agreement with an observation in Ref. [52], correcting a previous statement reported in Ref. [51].

III. ENTANGLEMENT MEASURE AND REFERENCE SYSTEM

In Refs. [47,48] QED scattering processes at tree-level are considered with disentangled incoming particles A and B in both cases with RR and RL initial helicity states. Then, after the scattering, the generated entanglement is quantified by using concurrence. In our setup, represented in Fig. 1, the scattering involves an electron A that collides with an entangled state formed by a positron B and an electron C. The scattering amplitudes and the spinors are described as functions of the scattering angle θ (see Appendixes A and B).

In order to better understand the generation and distribution of the entanglement, mediated by the QED interaction, we preliminary analyze the case of the (Bhabha) scattering of an electron A and a positron B in which the latter is in a superposition of helicity states [see Eq. (18) below]. This system will be used as a benchmark in Sec. IV to compare the generation and transfer of the entanglement in the various channels when the spectator particle C is added.

To calculate the concurrence, we use the definition as in Ref. [64],

$$C(\rho) = \max(0, \lambda_1 - \lambda_2 - \lambda_3 - \lambda_4), \tag{16}$$

where the λ_i, in decreasing order, are the square root of the eigenvalues of the matrix,

$$\mathcal{R} = \rho_{s_1 s_2} \tilde{\rho}_{s_1 s_2}, \tag{17}$$

with $\tilde{\rho}_{s_1 s_2} = (\sigma_y \otimes \sigma_y)\rho^*_{s_1 s_2}(\sigma_y \otimes \sigma_y)$, where σ_y is a Pauli matrix and s_1, s_2 are indices running in the bipartition subspaces.

Following the above discussion, we define our initial reference state as

$$|i\rangle_{\mathrm{REF}} = |R\rangle_A \otimes (\cos\eta |R\rangle_B + e^{i\beta}\sin\eta |L\rangle_B). \tag{18}$$

After the scattering, if we limit our attention to a selection of results at a fixed angle $\theta \neq 0, 2\pi$ we can express, up to a normalization factor,[2] the final reference state as

$$|f\rangle_{\mathrm{REF}} = \sum_{r,s=R,L} \left[\cos\eta \mathcal{M}(RR; rs)|r\rangle_A|s\rangle_B + e^{i\beta}\sin\eta \mathcal{M}(RL; rs)|r\rangle_A|s\rangle_B\right], \tag{19}$$

where the $\mathcal{M}(^{RR}_{LR}; rs)$ are the scattering amplitudes as reported in Appendix B. These correspond to the amplitudes given in Refs. [47,48].

By using Eqs. (18) and (19), we obtain the density matrices of initial and final reference state (omitting normalization factors),

$$\begin{aligned} \rho^i_{\mathrm{REF}} = \Big[&\cos^2\eta |R\rangle_A|R\rangle_{BB}\langle R|_A\langle R| + e^{-i\beta}\sin\eta\cos\eta |R\rangle_A|R\rangle_{BB}\langle L|_A\langle R| \\ &+ e^{i\beta}\sin\eta\cos\eta |R\rangle_A|L\rangle_{BB}\langle R|_A\langle R| + \sin^2\eta |R\rangle_A|L\rangle_{BB}\langle L|_A\langle R|\Big], \end{aligned} \tag{20}$$

$$\begin{aligned} \rho^f_{\mathrm{REF}} = \sum_{r,s,r',s'} \Big[&\cos^2\eta \mathcal{M}(RR, rs)\mathcal{M}^\dagger(RR, r's')|r\rangle_A|s\rangle_{BB}\langle s'|_A\langle r'| \\ &+ e^{-i\beta}\sin\eta\cos\eta \mathcal{M}(RR, rs)\mathcal{M}^\dagger(RL, r's')|r\rangle_A|s\rangle_{BB}\langle s'|_A\langle r'| \\ &+ e^{i\beta}\sin\eta\cos\eta \mathcal{M}(RL, rs)\mathcal{M}^\dagger(RR, r's')|r\rangle_A|s\rangle_{BB}\langle s'|_A\langle r'| \\ &+ \sin^2\eta \mathcal{M}(RL, rs)\mathcal{M}^\dagger(RL, r's')|r\rangle_A|s\rangle_{BB}\langle s'|_A\langle r'|\Big]. \end{aligned} \tag{21}$$

[2]The normalization can be fixed after the operation of momentum filtering (i.e., selection of the measurements relative to a specific scattering angle θ) that is formally described by applying a Positive-Operator Valued Measurement (POVM) as discussed in Ref. [50].

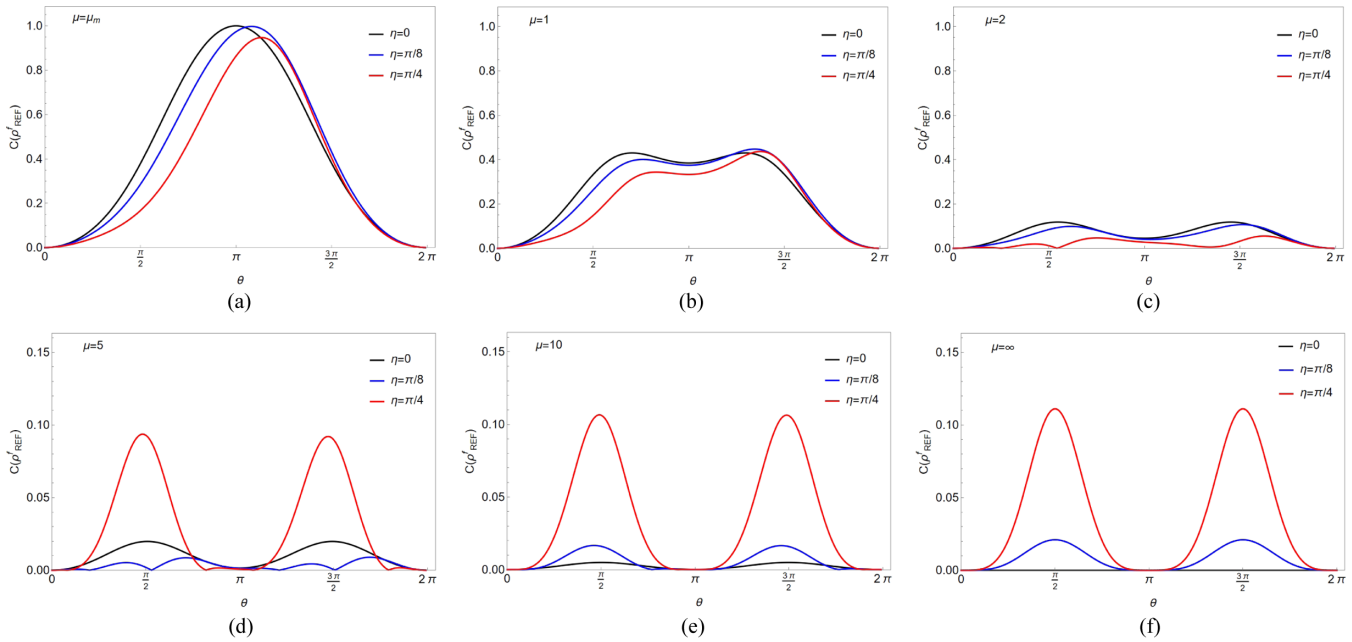

FIG. 2. Concurrence of reference state Eq. (21) from low momenta range shown in (a), (b), and (c), to high momenta range shown in (d), (f), and (g). Black lines correspond to the case reported in Ref. [47].

By using Eqs. (16) and (17) we calculate the amount of entanglement in the states ρ^i_{REF} and ρ^f_{REF}. For simplicity, we take the phase $\beta = 0$. The concurrence of the initial reference state vanishes, as expected. On the other hand, the concurrence of the final state is a cumbersome expression and it is not reported here. However, in the relativistic limit we obtain a simple form,

$$\lim_{\mu\to\infty} C(\rho^f_{\mathrm{REF}}) = \frac{2\sin^2\eta\sin^4(\theta/2)\cos^4(\theta/2)}{1-(1-\frac{1}{8}\sin^2\theta)\sin^2\theta\sin^2\eta}. \quad (22)$$

The fact that concurrence before the scattering is zero, means that the entanglement after the scattering is completely generated in the process. Some representative plots are reported in Fig. 2.

For the plots in Figs. 2(a)–2(f) we have chosen the following parameters; $\eta = \{0, \pi/8, \pi/4\}$ and $\mu = \{\mu_m \equiv \frac{1}{2}\sqrt{-3+\sqrt{17}}, 1, 2, 5, 10, 100\}$. The value of $\mu = \mu_m$ is the one for which the concurrence in the case of RR incoming particles ($\eta = 0$) is maximal. For this case we reproduce the results given in Refs. [47,48]. The other values of μ have been chosen to show the entanglement behavior from the nonrelativistic regime to the relativistic one ($\mu = 1$ corresponds to the characteristic scale for $|\vec{p}| = m_e$). On the other hand, $\eta = \pi/8$ and $\eta = \pi/4$ represent the cases in which the main features of the entanglement distribution for $\theta \in [0, 2\pi]$ become evident.

By increasing the momentum, for $\eta \neq 0$, the concurrence of our reference state shows a shift of its peak and an asymmetry with respect to $\theta = \pi$ emerges due to the interference terms in the associated density matrix. Moreover, from Figs. 2(a)–2(f) we can see that the concurrence value for $\eta = 0$ decreases and tends to zero in the relativistic limit, while for the other two cases $\eta = \pi/8$ and $\eta = \pi/4$, it increases and in the relativistic limit stabilizes its maxima at $\theta = \pi/2$ and $\theta = 3\pi/2$. These two values of η correspond to a change in the entanglement weight towards the case of $\eta = \pi/2$. In fact, by setting $\eta = \pi/2$ [see Fig. 3(a)], we recover the other case in Refs. [47,48] with R and L helicities for the incoming particles in which in the high-energy limit maximal entanglement emerges in $\theta = \pi/2$ and $\theta = 3\pi/2$. In the same limit, the other cases ($\eta \neq 0,\ \pi/2$) show that the asymmetry in concurrence with respect to $\theta = \pi$ is suppressed. We remark that this asymmetry, as shown in Figs. 3(b)–3(c), is due to the choice of initial polarizations; for different incoming helicity states, the amplitudes $\mathcal{M}(RR, rs)$ and $\mathcal{M}(RL, rs)$ carry different weights to the final concurrence. Choosing the opposite polarizations for A and B, we recover the reflected plot with respect to $\theta = \pi$.

In order to better understand the generation of entanglement and its dependence on the scattering angle θ, we can look at the relation between concurrence and the probabilities associated to the four output helicity states; when, for some parameter configurations, one of these probabilities is equal to 1, no entanglement can be generated. On the other hand, the concurrence is maximal in correspondence of equal output probabilities of two of the four final states. These cases correspond to the possible Bell states that can be formed only in the special cases for $\eta = 0$, $\mu = \mu_m$,

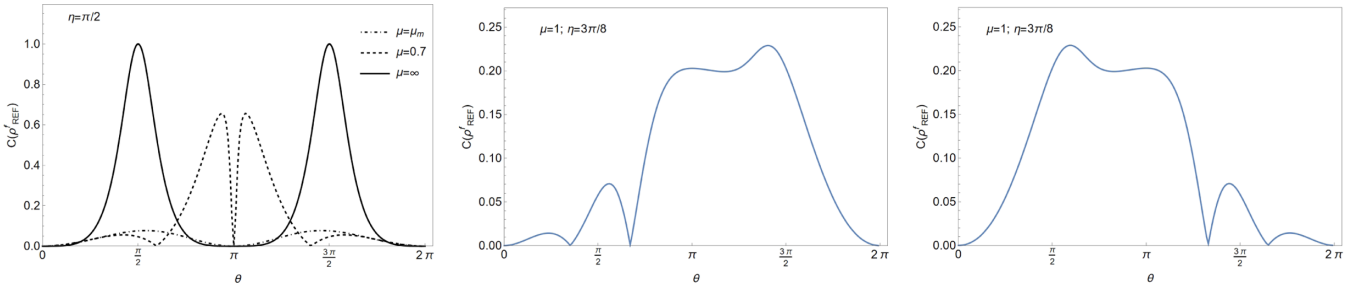

(a) (b) (c)

FIG. 3. (a) Concurrence of reference state Eq. (21) for incoming RL helicities and different values of μ with $\eta = \pi/2$. In the high-energy limit maximal entanglement is generated for $\theta = \pi/2, 3\pi/2$ (see also Ref. [47]). (b) Concurrence of reference state Eq. (21). (c) Concurrence of reference state Eq. (21) with opposite helicities for incoming particles.

$\theta = \pi$ and for $\eta = \pi/2$, $\mu = \infty$, $\theta = \pi/2, 3\pi/2$. Other situations, corresponding to different parameter configurations, are the consequence of the interplay between the $\eta = 0$ and $\eta = \pi/2$ initial states.

IV. ENTANGLEMENT DISTRIBUTION IN BIPARTITE SUBSYSTEMS

In Sec. III we studied an extension of the setup considered in Refs. [47,48,50], in which we have considered the positron B in a superposition of helicity states as in Eq. (18). Now we come back to the original system, where a spectator particle C (electron) is entangled with the positron B which scatters with the electron A as represented pictorially in Fig. 1. The states before and after the scattering are expressed by

$$|i\rangle = |R\rangle_A \otimes (\cos\eta|R\rangle_B|R\rangle_C + e^{i\beta}\sin\eta|L\rangle_B|L\rangle_C), \tag{23}$$

and

$$|f\rangle = \sum_{r,s=R,L}\left[\cos\eta\mathcal{M}(RR;rs)|r\rangle_A|s\rangle_B|R\rangle_C + e^{i\beta}\sin\eta\mathcal{M}(RL;rs)|r\rangle_A|s\rangle_B|L\rangle_C\right]. \tag{24}$$

From Eqs. (23) and (24) we can calculate the density matrices of the system. We obtain (omitting normalization factors),

$$\begin{aligned}\rho^i_{ABC} = {} & \cos^2\eta|R\rangle_A|R\rangle_B|R\rangle_{CC}\langle R|_B\langle R|_A\langle R| + e^{-i\beta}\sin\eta\cos\eta|R\rangle_A|R\rangle_B|R\rangle_{CC}\langle L|_B\langle L|_A\langle R| \\ & + e^{i\beta}\sin\eta\cos\eta|R\rangle_A|L\rangle_B|L\rangle_{CC}\langle R|_B\langle R|_A\langle R| + \sin^2\eta|R\rangle_A|L\rangle_B|L\rangle_{CC}\langle L|_B\langle L|_A\langle R|,\end{aligned} \tag{25}$$

$$\begin{aligned}\rho^f_{ABC} = {} & \sum_{r,s,r',s'}\left[\cos^2\eta\mathcal{M}(RR,rs)\mathcal{M}^\dagger(RR,r's')|r\rangle_A|s\rangle_B|R\rangle_{CC}\langle R|_B\langle s'|_A\langle r'| \right. \\ & + e^{-i\beta}\sin\eta\cos\eta\mathcal{M}(RR,rs)\mathcal{M}^\dagger(RL,r's')|r\rangle_A|s\rangle_B|R\rangle_{CC}\langle L|_B\langle s'|_A\langle r'| \\ & + e^{i\beta}\sin\eta\cos\eta\mathcal{M}(RL,rs)\mathcal{M}^\dagger(RR,r's')|r\rangle_A|s\rangle_B|L\rangle_{CC}\langle R|_B\langle s'|_A\langle r'| \\ & \left. + \sin^2\eta\mathcal{M}(RL,rs)\mathcal{M}^\dagger(RL,r's')|r\rangle_A|s\rangle_B|L\rangle_{CC}\langle L|_B\langle s'|_A\langle r'|\right].\end{aligned} \tag{26}$$

By tracing with respect to A, B, C, the resulting reduced density matrices are

$$\rho^i_{AB} = \cos^2\eta|R\rangle_A|R\rangle_{BB}\langle R|_A\langle R| + \sin^2\eta|R\rangle_A|L\rangle_{BB}\langle L|_A\langle R|, \tag{27}$$

$$\rho^i_{AC} = \cos^2\eta|R\rangle_A|R\rangle_{CC}\langle R|_A\langle R| + \sin^2\eta|R\rangle_A|L\rangle_{CC}\langle L|_A\langle R|, \tag{28}$$

$$\begin{aligned}\rho^i_{BC} = {} & \cos^2\eta|R\rangle_B|R\rangle_{CC}\langle R|_B\langle R| + e^{-i\beta}\sin\eta\cos\eta|R\rangle_B|R\rangle_{CC}\langle L|_B\langle L| \\ & + e^{i\beta}\sin\eta\cos\eta|L\rangle_B|L\rangle_{CC}\langle R|_B\langle R| + \sin^2\eta|L\rangle_B|L\rangle_{CC}\langle L|_B\langle L|,\end{aligned} \tag{29}$$

$$\rho^f_{AB} = \sum_{r,s,r',s'} \big[\cos^2\eta \mathcal{M}(RR;rs)\mathcal{M}^\dagger(RR;r's')|r\rangle_A|s\rangle_{BB}\langle s'|_A\langle r'| + \sin^2\eta \mathcal{M}(RL;rs)\mathcal{M}^\dagger(RL;r's')|r\rangle_A|s\rangle_{BB}\langle s'|_A\langle r'|\big], \tag{30}$$

$$\rho^f_{AC} = \sum_{r,r',s} \big[\cos^2\eta \mathcal{M}(RR;rs)\mathcal{M}^\dagger(RR;r's)|r\rangle_A|R\rangle_{CC}\langle R|_A\langle r'| + e^{-i\beta}\sin\eta\cos\eta \mathcal{M}(RR;rs)\mathcal{M}^\dagger(RL;r's)|r\rangle_A|R\rangle_{CC}\langle L|_A\langle r'| + e^{i\beta}\sin\eta\cos\eta \mathcal{M}(RL;rs)\mathcal{M}^\dagger(RR;r's)|r\rangle_A|L\rangle_{CC}\langle R|_A\langle r'| + \sin^2\eta \mathcal{M}(RL;rs)\mathcal{M}^\dagger(RL;r's)|r\rangle_A|L\rangle_{CC}\langle L|_A\langle r'|\big], \tag{31}$$

$$\rho^f_{BC} = \sum_{r,r,s'} \big[\cos^2\eta \mathcal{M}(RR;rs)\mathcal{M}^\dagger(RR;rs')|s\rangle_B|R\rangle_{CC}\langle R|_B\langle s'| + e^{-i\beta}\sin\eta\cos\eta \mathcal{M}(RR;rs)\mathcal{M}^\dagger(RL;rs')|s\rangle_B|R\rangle_{CC}\langle L|_B\langle s'| + e^{i\beta}\sin\eta\cos\eta \mathcal{M}(RL;rs)\mathcal{M}^\dagger(RR;rs')|s\rangle_B|L\rangle_{CC}\langle R|_B\langle s'| + \sin^2\eta \mathcal{M}(RL;rs)\mathcal{M}^\dagger(RL;rs')|s\rangle_B|L\rangle_{CC}\langle L|_B\langle s'|\big]. \tag{32}$$

Using Eqs. (16) and (17) we calculate the concurrence associated to each of the six bipartite systems (27)–(32). As before, we take $\beta = 0$. For the bipartitions of the initial state, we obtain $C(\rho^i_{AB}) = 0$, $C(\rho^i_{AC}) = 0$ and $C(\rho^i_{BC}) = |\sin(2\eta)|$. On the other hand, the expressions of concurrence for the bipartitions of the final states are very lengthy and they are not reported here except for those in the relativistic limit, that we list below:

$$\lim_{\mu\to\infty} C(\rho^f_{AB}) = \frac{2\sin^2\eta\sin^4(\theta/2)\cos^4(\theta/2)}{1-(1-\frac{1}{8}\sin^2\theta)\sin^2\theta\sin^2\eta}, \tag{33}$$

$$\lim_{\mu\to\infty} C(\rho^f_{AC}) = \frac{\sin(2\eta)\sin^4(\theta/2)}{1-(1-\frac{1}{8}\sin^2\theta)\sin^2\theta\sin^2\eta}, \tag{34}$$

$$\lim_{\mu\to\infty} C(\rho^f_{BC}) = \frac{\sin(2\eta)\cos^4(\theta/2)}{1-(1-\frac{1}{8}\sin^2\theta)\sin^2\theta\sin^2\eta}. \tag{35}$$

Some representative plots of concurrences numerically evaluated are reported in Figs. 4–6. For each set of plots, we have chosen four values of μ: $\{\mu_m, 1, 5, 100\}$ and η: $\{0, \pi/8, \pi/4, 3\pi/8\}$, which are sufficient to clearly represent the generation and distribution of the entanglement in the three channels AB, AC, and BC. The plots (a)–(f) in each figure represent the concurrence as a function of the scattering angle θ.

In each set corresponding to $\eta = \pi/8$ and $\eta = \pi/4$ in Figs. 4–5, the concurrence in the BC channel decreases with respect to its initial value while in the AC channel increases. On the other hand, in the same range of parameters, concurrence in the AB channel has a nontrivial behavior, which however stabilizes in the relativistic limit for $\theta = \frac{1}{2}\pi$ and $\theta = \frac{3}{2}\pi$, where it is maximal as for the (initial) disentangled case $\eta = \pi/2$ (i.e. with RL incoming polarization particles) as reported in [47] and in Sec. III. We find remarkable that the correlation between the two particles A and C that not interact directly increases as a consequence of the scattering between A and B.

On the other hand, when we consider the cases for $\eta > \pi/4$ up to $\eta = \frac{3}{4}\pi$, entanglement in the BC channel may also increase with respect to its initial value. This is clear from Fig. 6(c) and Fig. 6(f) which show the particular case $\eta = \frac{3}{8}\pi$.

Let us consider now the relativistic limit, in which the analytic expressions Eqs. (33)–(35) for the concurrences are available. We observe that in such a limit, the entanglement in the AB channel Eq. (33) is identical to the one for the reference state Eq. (22); thus, it appears to be completely generated in the scattering process.

We now further specialize to the particular case of $\eta = \pi/4$, corresponding to maximal entanglement for the initial state BC. From Eq. (34), we see that at $\theta = \pi$, the entanglement in the AC output channel is maximal, while it vanishes in the BC output channel. Thus the QED scattering between A and B acts as a quantum gate for the complete transfer of the entanglement between AC and BC.

We also notice that correspondingly, the entanglement generated in the scattering assumes low values, thus entanglement transfer is a dominant and stable mechanism

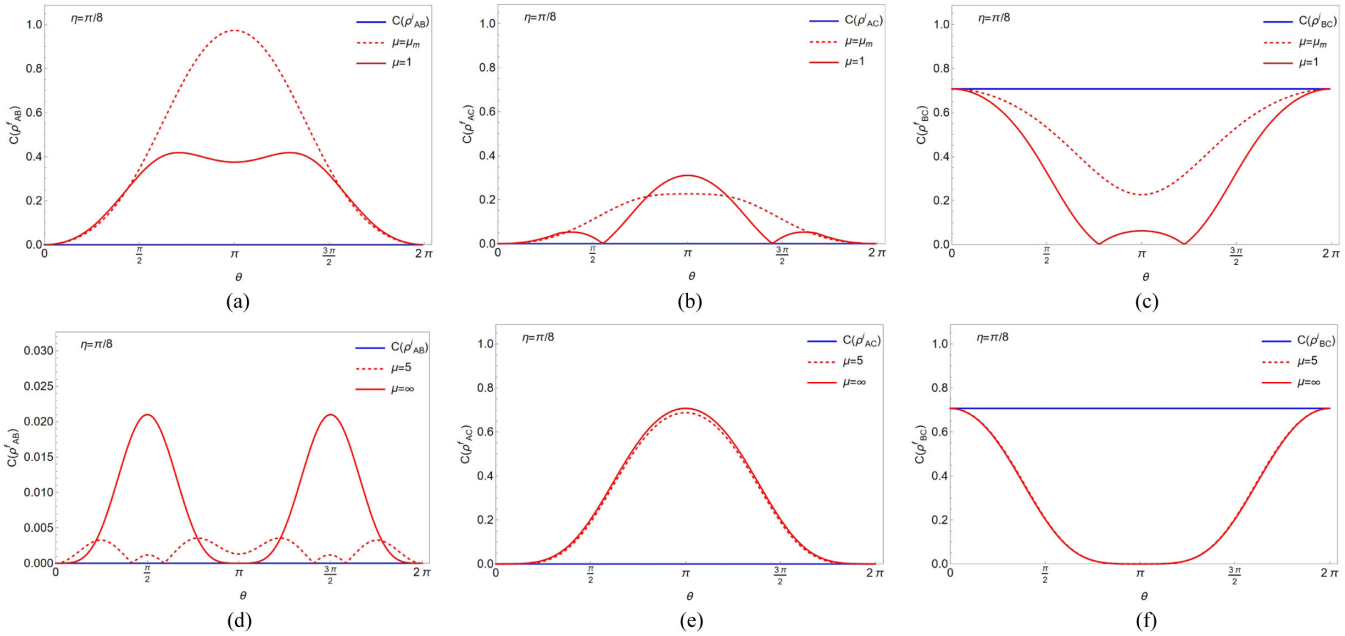

FIG. 4. Concurrence of final bipartitions for $\eta = \pi/8$.

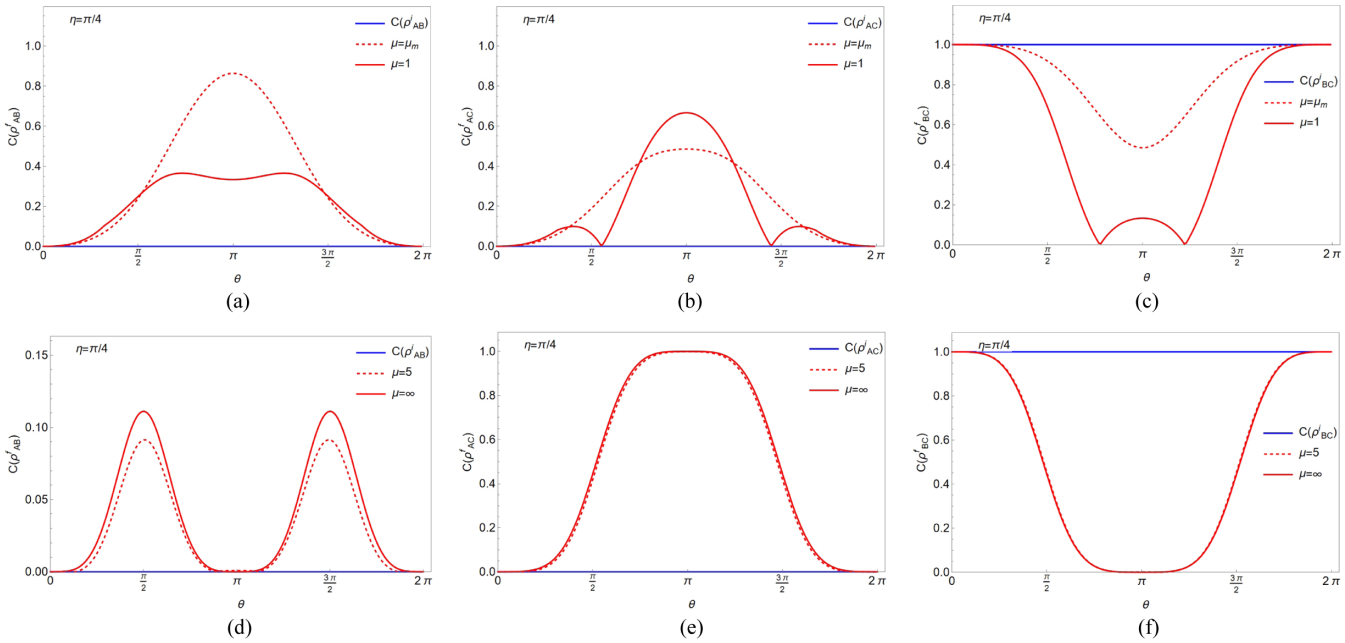

FIG. 5. Concurrence of final bipartitions for $\eta = \pi/4$.

around $\theta = \pi$ in the relativistic limit and for entanglement weight $\eta = \pi/4$.

Finally, we comment on the interpretation of these results in terms of output probabilities, in a similar way as done in Sec. III. Here we note that the presence of the spectator implies the suppression of interference terms in the expressions for probabilities and concurrence: this is the reason for the symmetry of the plots Figs. 4–6 with respect to those in Figs. 2–3. Also, we observe that a Bell state cannot be generated in the AB channel, due to the fact that $\eta \neq 0, \pi/2$.

V. CONCLUSIONS AND OUTLOOK

In this work, we have studied entanglement in the context of QED processes. In particular, we have considered Bhabha scattering at tree-level in which a positron B, that scatters with an electron A, is entangled in spin with

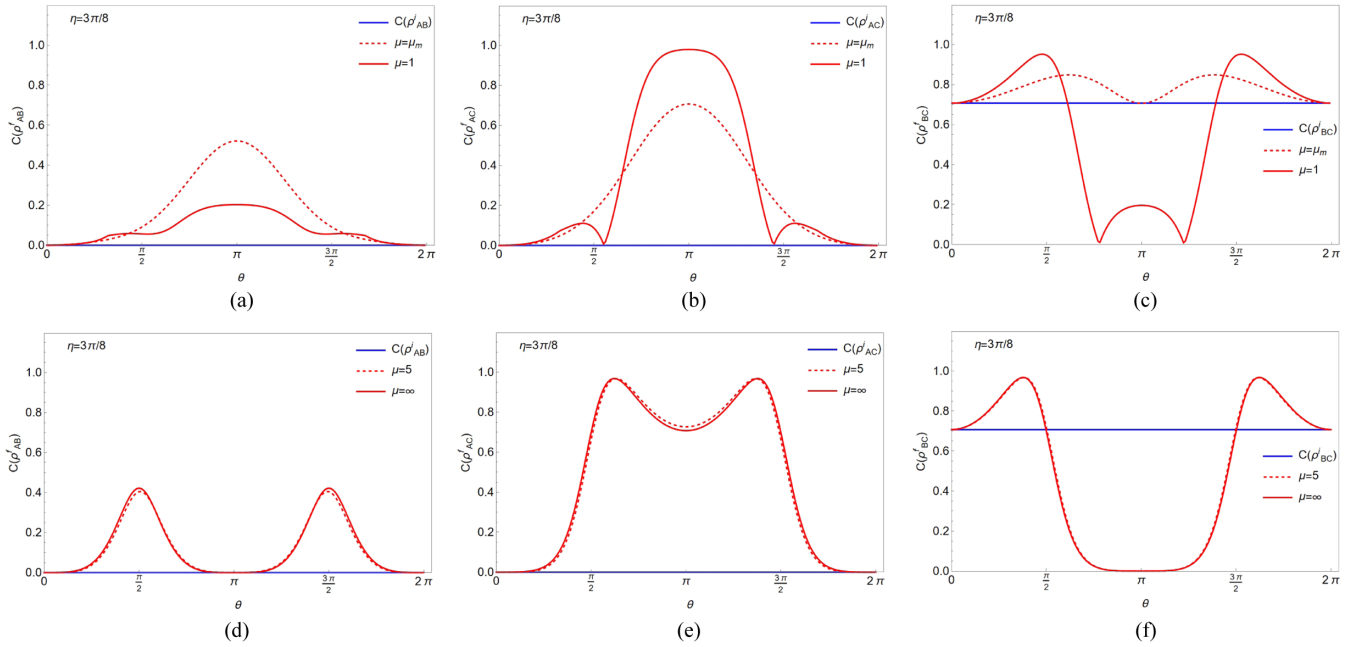

FIG. 6. Concurrence of final bipartitions for $\eta = 3\pi/8$.

another electron C that does not participate directly in the process. We found that two effects occur; the entanglement generation at the interaction vertex and the distribution of the initial entanglement among the three channels.

By using the concurrence, we have quantified the entanglement in the three bipartitions of the system: AB, AC, and BC—before and after the scattering. The correlations depend on the value of the entanglement weight η, the scattering angle θ, and the ratio between the incoming momentum and the mass μ. The interplay between generation and transfer of entanglement among the three channels is very complex in the nonrelativistic regime, namely for $\mu \simeq 1$. On the other hand, for some configurations of parameters, the entanglement tends to concentrate in some bipartitions.

Especially interesting is the relativistic regime $\mu = \infty$. In such a limit, we were able to calculate the analytic expressions for the concurrences and found that the entanglement in the AB output channel is not affected by the presence of the entangled spectator particle, thus being completely generated in the scattering. On the other hand, for $\eta = \pi/4$, we observe a complete transfer of entanglement from the BC channel to the AC channel in a neighbor of $\theta = \pi$. In this situation, the QED scattering between A and B acts as a quantum gate for such a transfer between AC and BC. It is an intriguing question if such a mechanism could be useful for quantum information tasks.

This work represents a contribution towards a better understanding of the underlying mechanisms in the generation and distribution of the entanglement in the framework of fundamental interactions. A first extension of the present analysis, which is in progress, is represented by the detailed study of other basic QED scattering processes (Möller, Compton). We also plan to carry out the same investigation in different reference frames, also to test the Lorentz invariance of our results. Another important issue, which we have not considered in this work, is the study of tripartite entanglement in the output state; this will be also useful to understand the balance in the generation and transfer of the entanglement in the process, which does not appear to satisfy a simple sum rule.

ACKNOWLEDGMENTS

M. B. wishes to thank Francesco Romeo for illuminating discussions. B. M. is grateful to Cristina Matrella, Gennaro Zanfardino, Pasquale Bosso, and Gaetano Luciano for fruitful conversations on many topics related to the paper.

APPENDIX A:

1. Weyl representation of γ-matrices

$$\gamma^0 = \begin{pmatrix} 0 & \mathbb{1} \\ \mathbb{1} & 0 \end{pmatrix}, \quad \gamma^i = \begin{pmatrix} 0 & \sigma^i \\ -\sigma^i & 0 \end{pmatrix}, \quad \gamma^5 = \begin{pmatrix} -\mathbb{1} & 0 \\ 0 & \mathbb{1} \end{pmatrix}. \tag{A1}$$

Dirac spinors, as in Ref. [65], correspond to the particle and antiparticle solutions of the Dirac equations,

$$(\gamma^\mu p_\mu - m)u(p,s) = 0, \tag{A2}$$

$$(\gamma^\mu p_\mu + m)v(p,s) = 0. \tag{A3}$$

They can be written as

$$u(p,s) = \begin{pmatrix} \sqrt{p\cdot\sigma}\xi^s \\ \sqrt{p\cdot\bar{\sigma}}\xi^s \end{pmatrix}, \qquad v(p,s) = \begin{pmatrix} \sqrt{p\cdot\sigma}\xi^s \\ -\sqrt{p\cdot\bar{\sigma}}\xi^s \end{pmatrix}, \tag{A4}$$

where the ξ^s are the two component spinors eigenstates of helicity operator, $\sigma = (\mathbb{1}, \vec{\sigma})$, $\bar{\sigma} = (\mathbb{1}, -\vec{\sigma})$ in which $\vec{\sigma}$ represents the Pauli matrices and $p = (\omega, \vec{p})$ is the 4-momentum vector. The spinors below are expressed in terms of an arbitrary direction in which $\vec{p} = (\sin\theta\cos\phi, \sin\theta\sin\phi, \cos\theta)$, with θ, ϕ the polar angles, and the subscripts R and L represent respectively the positive $(+1)$ and negative (-1) eigenvalues of the helicity operator.

2. Helicity spinors

$$u_R(\vec{p}) = \begin{pmatrix} \sqrt{\omega-p}\cos\left(\frac{\theta}{2}\right) \\ \sqrt{\omega-p}e^{i\phi}\sin\left(\frac{\theta}{2}\right) \\ \sqrt{\omega+p}\cos\left(\frac{\theta}{2}\right) \\ \sqrt{\omega+p}e^{i\phi}\sin\left(\frac{\theta}{2}\right) \end{pmatrix}, \qquad u_L(\vec{p}) = \begin{pmatrix} -\sqrt{\omega+p}\sin\left(\frac{\theta}{2}\right) \\ \sqrt{\omega+p}e^{i\phi}\cos\left(\frac{\theta}{2}\right) \\ -\sqrt{\omega-p}\sin\left(\frac{\theta}{2}\right) \\ \sqrt{\omega-p}e^{i\phi}\cos\left(\frac{\theta}{2}\right) \end{pmatrix}, \tag{A5}$$

$$v_R(\vec{p}) = \begin{pmatrix} -\sqrt{\omega+p}\sin\left(\frac{\theta}{2}\right) \\ \sqrt{\omega+p}e^{i\phi}\cos\left(\frac{\theta}{2}\right) \\ \sqrt{\omega-p}\sin\left(\frac{\theta}{2}\right) \\ -\sqrt{\omega-p}e^{i\phi}\cos\left(\frac{\theta}{2}\right) \end{pmatrix}, \qquad v_L(\vec{p}) = \begin{pmatrix} \sqrt{\omega-p}\cos\left(\frac{\theta}{2}\right) \\ \sqrt{\omega-p}e^{i\phi}\sin\left(\frac{\theta}{2}\right) \\ -\sqrt{\omega+p}\cos\left(\frac{\theta}{2}\right) \\ -\sqrt{\omega+p}e^{i\phi}\sin\left(\frac{\theta}{2}\right) \end{pmatrix}, \tag{A6}$$

$$u_R(-\vec{p}) = \begin{pmatrix} -\sqrt{\omega-p}\sin\left(\frac{\theta}{2}\right) \\ \sqrt{\omega-p}e^{i\phi}\cos\left(\frac{\theta}{2}\right) \\ -\sqrt{\omega+p}\sin\left(\frac{\theta}{2}\right) \\ \sqrt{\omega+p}e^{i\phi}\cos\left(\frac{\theta}{2}\right) \end{pmatrix}, \qquad u_L(-\vec{p}) = \begin{pmatrix} \sqrt{\omega+p}\cos\left(\frac{\theta}{2}\right) \\ \sqrt{\omega+p}e^{i\phi}\sin\left(\frac{\theta}{2}\right) \\ \sqrt{\omega-p}\cos\left(\frac{\theta}{2}\right) \\ \sqrt{\omega-p}e^{i\phi}\sin\left(\frac{\theta}{2}\right) \end{pmatrix}, \tag{A7}$$

$$v_R(-\vec{p}) = \begin{pmatrix} \sqrt{\omega+p}\cos\left(\frac{\theta}{2}\right) \\ \sqrt{\omega+p}e^{i\phi}\sin\left(\frac{\theta}{2}\right) \\ -\sqrt{\omega-p}\cos\left(\frac{\theta}{2}\right) \\ -\sqrt{\omega-p}e^{i\phi}\sin\left(\frac{\theta}{2}\right) \end{pmatrix}, \qquad v_L(-\vec{p}) = \begin{pmatrix} -\sqrt{\omega-p}\sin\left(\frac{\theta}{2}\right) \\ \sqrt{\omega-p}e^{i\phi}\cos\left(\frac{\theta}{2}\right) \\ \sqrt{\omega+p}\sin\left(\frac{\theta}{2}\right) \\ -\sqrt{\omega+p}e^{i\phi}\cos\left(\frac{\theta}{2}\right) \end{pmatrix}. \tag{A8}$$

APPENDIX B: BHABHA SCATTERING AMPLITUDES

The scattering amplitudes are calculated in the COM reference frame of particles A and B. In the following, $p_1 = (\omega, 0, 0, |\vec{p}|)$ and $p_2 = (\omega, 0, 0, -|\vec{p}|)$ are the incoming 4-momenta that lie along the z-axis, while $p_3 = (\omega, |\vec{p}|\sin\theta, 0, |\vec{p}|\cos\theta)$ and $p_4 = (\omega, -|\vec{p}|\sin\theta, 0, -|\vec{p}|\cos\theta))$ are the outgoing 4-momenta lying along a direction that form an angle θ with respect to z-axis. a, b, r, s are the spin indices,

$$\mathcal{M}_{\text{Bhabha}} = e^2\left(\bar{v}(b,p_2)\gamma^\mu u(a,p_1)\frac{1}{(p_1+p_2)^2}\bar{u}(r,p_3)\gamma_\mu v(s,p_4) - \bar{v}(b,p_2)\gamma^\mu v(s,p_4)\frac{1}{(p_3-p_1)^2}\bar{u}(r,p_3)\gamma_\mu u(a,p_1)\right). \tag{B1}$$

Defining $\mu \equiv \frac{|\mathbf{p}|}{m_e}$, where $|\mathbf{p}|$ is the incoming momentum in the COM reference frame and m_e the electron mass, the explicit expressions for the polarized amplitudes result,

$$\mathcal{M}(RR;RR) = \mathcal{M}(LL;LL) = \frac{(2+11\mu^2+8\mu^4+2\cos\theta+\mu^2\cos 2\theta)\csc^2(\frac{\theta}{2})}{4\mu^2(1+\mu^2)}, \tag{B2}$$

$$\mathcal{M}(RR;{}^{RL}_{LR}) = -\mathcal{M}(LL;{}^{RL}_{LR}) = -\frac{(1+\mu^2\cos\theta)\cot(\frac{\theta}{2})}{\mu^2\sqrt{1+\mu^2}}, \tag{B3}$$

$$\mathcal{M}(RR;LL) = \mathcal{M}(LL;RR) = \frac{1+\mu^2(1+\cos\theta)}{\mu^2(1+\mu^2)}, \tag{B4}$$

$$\mathcal{M}({}^{RL}_{LR};RR) = -\mathcal{M}({}^{RL}_{LR};LL) = \frac{(1+\mu^2\cos\theta)\cot(\frac{\theta}{2})}{\mu^2\sqrt{1+\mu^2}}, \tag{B5}$$

$$\mathcal{M}(RL;RL) = \mathcal{M}(LR;LR) = \frac{(1+\mu^2(1+\cos\theta))\cot^2(\frac{\theta}{2})}{\mu^2}, \tag{B6}$$

$$\mathcal{M}(RL;LR) = \mathcal{M}(LR;RL) = 1-\cos\theta-\frac{1}{\mu^2}. \tag{B7}$$

[1] R. A. Bertlmann and B. C. Hiesmayr, Bell inequalities for entangled kaons and their unitary time evolution, Phys. Rev. A **63**, 062112 (2001).

[2] R. A. Bertlmann, W. Grimus, and B. C. Hiesmayr, Bell inequality and *CP* violation in the neutral kaon system, Phys. Lett. A **289**, 21 (2001).

[3] L. Lello, D. Boyanovsky, and R. Holman, Entanglement entropy in particle decay, J. High Energy Phys. 11 (2013) 116.

[4] J. Bernabeu, T and *CPT* symmetries in entangled neutral meson systems, J. Phys. Conf. Ser. **335**, 012011 (2011).

[5] S. Seki and S. J. Sin, EPR = ER, scattering amplitude and entanglement entropy change, Phys. Lett. B **735**, 272 (2014).

[6] R. Peschanski and S. Seki, Entanglement entropy of scattering particles, Phys. Lett. B **758**, 89 (2016).

[7] M. Blasone, F. Dell'Anno, S. De Siena, M. Di Mauro, and F. Illuminati, Multipartite entangled states in particle mixing, Phys. Rev. D **77**, 096002 (2008).

[8] M. Blasone, F. Dell'Anno, S. De Siena, and F. Illuminati, A field-theoretical approach to entanglement in neutrino mixing and oscillations, Europhys. Lett. **106**, 30002 (2014).

[9] M. Blasone, F. Dell'Anno, S. De Siena, and F. Illuminati, Entanglement in a QFT model of neutrino oscillations, Adv. High Energy Phys. **2014**, 359168 (2014).

[10] V. A. S. V. Bittencourt, M. Blasone, and G. Zanfardino, Chiral and flavor oscillations in lepton-antineutrino spin correlations, J. Phys. Conf. Ser. **2533**, 012024 (2023).

[11] V. A. S. V. Bittencourt, M. Blasone, F. Illuminati, G. Lambiase, G. G. Luciano, and L. Petruzziello, Quantum nonlocality in extended theories of gravity, Phys. Rev. D **103**, 044051 (2021).

[12] A. Iorio, G. Lambiase, and G. Vitiello, Entangled quantum fields near the event horizon and entropy, Ann. Phys. (Amsterdam) **309**, 151 (2004).

[13] A. K. Alok, S. Banerjee, and S. U. Sankar, Quantum correlations in terms of neutrino oscillation probabilities, Nucl. Phys. **B909**, 65 (2016).

[14] E. B. Manoukian and N. Yongram, Speed dependent polarization correlations in QED and entanglement, Eur. Phys. J. D **31**, 137 (2004).

[15] N. Yongram, E. B. Manoukian, and S. Siranan, Polarization correlations in muon pair production in the electroweak model, Mod. Phys. Lett. A **21**, 979 (2006).

[16] N. Yongram, Spin correlations in e^+e^- pair creation by two-photons and entanglement in QED, Int. J. Theor. Phys. **50**, 838 (2011).

[17] S. Banerjee, A. K. Alok, R. Srikanth, and B. C. Hiesmayr, A quantum information theoretic analysis of three flavor neutrino oscillations, Eur. Phys. J. C **75**, 487 (2015).

[18] D. Gangopadhyay, D. Home, and A. S. Roy, Probing the Leggett-Garg inequality for oscillating neutral kaons and neutrinos, Phys. Rev. A **88**, 022115 (2013).

[19] D. Gangopadhyay and A. S. Roy, Three-flavoured neutrino oscillations and the Leggett–Garg inequality, Eur. Phys. J. C **77**, 260 (2017).

[20] J. A. Formaggio, D. I. Kaiser, M. M. Murskyj, and T. E. Weiss, Violation of the Leggett-Garg inequality in neutrino oscillations, Phys. Rev. Lett. **117**, 050402 (2016).
[21] J. Naikoo, A. Kumar Alok, S. Banerjee, and S. Uma Sankar, Leggett-Garg inequality in the context of three flavour neutrino oscillation, Phys. Rev. D **99**, 095001 (2019).
[22] J. Naikoo, A. K. Alok, S. Banerjee, S. Uma Sankar, G. Guarnieri, C. Schultze, and B. C. Hiesmayr, A quantum information theoretic quantity sensitive to the neutrino mass-hierarchy, Nucl. Phys. **B951**, 114872 (2020).
[23] M. Blasone, F. Illuminati, L. Petruzziello, and L. Smaldone, Leggett-Garg inequalities in the quantum field theory of neutrino oscillations, Phys. Rev. A **108**, 032210 (2023).
[24] M. Blasone, F. Illuminati, L. Petruzziello, K. Simonov, and L. Smaldone, No-signaling-in-time as a condition for macrorealism: the case of neutrino oscillations, Eur. Phys. J. C **83**, 688 (2023).
[25] X. Z. Wang and B. Q. Ma, New test of neutrino oscillation coherence with Leggett–Garg inequality, Eur. Phys. J. C **82**, 133 (2022).
[26] X. K. Song, Y. Huang, J. Ling, and M. H. Yung, Quantifying quantum coherence in experimentally-observed neutrino oscillations, Phys. Rev. A **98**, 050302 (2018).
[27] R. Uola, A. C. S. Costa, H. Chau Nguyen, and O. Uühne, Quantum steering, Rev. Mod. Phys. **92**, 015001 (2020).
[28] K. Dixit, J. Naikoo, S. Banerjee, and A. Kumar Alok, Study of coherence and mixedness in meson and neutrino systems, Eur. Phys. J. C **79**, 96 (2019).
[29] F. Ming, X. K. Song, J. Ling, L. Ye, and D. Wang, Quantification of quantumness in neutrino oscillations, Eur. Phys. J. C **80**, 275 (2020).
[30] Y. W. Li, L. J. Li, X. K. Song, and D. Wang, Trade-off relations of quantum resource theory in neutrino oscillations, Eur. Phys. J. Plus **137**, 1267 (2022).
[31] M. Blasone, S. De Siena, and C. Matrella, Wave packet approach to quantum correlations in neutrino oscillations, Eur. Phys. J. C **81**, 660 (2021).
[32] D. Wang, F. Ming, X. K. Song, L. Ye, and J. L. Chen, Entropic uncertainty relation in neutrino oscillations, Eur. Phys. J. C **80**, 800 (2020).
[33] M. Blasone, S. De Siena, and C. Matrella, Non-locality and entropic uncertainty relations in neutrino oscillations, Eur. Phys. J. Plus **137**, 1272 (2022).
[34] S. R. Beane, D. B. Kaplan, N. Klco, and M. J. Savage, Entanglement suppression and emergent symmetries of strong interactions, Phys. Rev. Lett. **122**, 102001 (2019).
[35] R. Aoude, M. Z. Chung, Y. T. Huang, C. S. Machado, and M. K. Tam, Silence of binary Kerr black holes, Phys. Rev. Lett. **125**, 181602 (2020).
[36] I. Low and T. Mehen, Symmetry from entanglement suppression, Phys. Rev. D **104**, 074014 (2021).
[37] D. E. Kharzeev and E. M. Levin, Deep inelastic scattering as a probe of entanglement, Phys. Rev. D **95**, 114008 (2017).
[38] J. Fan and X. Li, Relativistic effect of entanglement in fermion-fermion scattering, Phys. Rev. D **97**, 016011 (2018).
[39] M. Blasone, S. De Siena, G. Lambiase, C. Matrella, and B. Micciola, Complete complementarity relations in tree level QED processes, arXiv:2402.09195.
[40] Y. Afik and J. R. M. de Nova, Entanglement and quantum tomography with top quarks at the LHC, Eur. Phys. J. Plus **136**, 907 (2021).
[41] Y. Afik and J. R. M. de Nova, Quantum information with top quarks in QCD, Quantum **6**, 820 (2022).
[42] Y. Afik and J. R. M. de Nova, Quantum discord and steering in top quarks at the LHC, Phys. Rev. Lett. **130**, 221801 (2023).
[43] C. Severi, C. D. Boschi, F. Maltoni, and M. Sioli, Quantum tops at the LHC: from entanglement to Bell inequalities, Eur. Phys. J. C **82**, 285 (2022).
[44] T. Han, M. Low, and T. A. Wu, Quantum entanglement and Bell inequality violation in semi-leptonic top decays, arXiv:2310.17696.
[45] M. Ghodrati, String amplitudes and mutual information in confining backgrounds: The partonic behavior, arXiv:2307.13454.
[46] S. Fedida, A. Mazumdar, S. Bose, and A. Serafini, Entanglement entropy in scalar quantum electrodynamics,3 Phys. Rev. D **109**, 065028 (2024).
[47] A. Cervera-Lierta, J. I. Latorre, J. Rojo, and L. Rottoli, Maximal entanglement in high energy physics, SciPost Phys. **3**, 036 (2017).
[48] A. Cervera Lierta, Maximal entanglement: Applications in quantum information and particle physics, arXiv:1906.12099.
[49] R. Peschanski and S. Seki, Entanglement entropy of scattering particles, Phys. Lett. B **758**, 89 (2016).
[50] S. Fedida and A. Serafini, Tree-level entanglement in quantum electrodynamics, Phys. Rev. D **107**, 116007 (2023).
[51] J. B. Araujo, B. Hiller, I. G. da Paz, Manoel M. Ferreira, Marcos Sampaio, and H. A. S. Costa, Measuring QED cross sections via entanglement, Phys. Rev. D **100**, 105018 (2019).
[52] J. D. Fonseca, B. Hiller, J. B. Araujo, I. G. da Paz, and M. Sampaio, Entanglement and scattering in quantum electrodynamics: S matrix information from an entangled spectator particle, Phys. Rev. D **106**, 056015 (2022).
[53] J. Fan, G. M. Deng, and X. J. Ren, Entanglement entropy and monotones in scattering process, Phys. Rev. D **104**, 116021 (2021).
[54] S. Shivashankara, Entanglement entropy of Compton scattering with a witness, Can. J. Phys. **101**, 757 (2023).
[55] G. M. Quinta and R. André, Multipartite entanglement from consecutive scatterings, Phys. Rev. A **109**, 022433 (2024).
[56] R. A. Morales, Exploring Bell inequalities and quantum entanglement in vector boson scattering, Eur. Phys. J. Plus **138**, 1157 (2023).
[57] G. A. Miller, Entanglement maximization in low-energy neutron-proton scattering, Phys. Rev. C **108**, L031002 (2023).
[58] G. A. Miller, Entanglement of elastic and inelastic scattering, Phys. Rev. C **108**, L041601 (2023).
[59] A. Pérez-Obiol, S. Masot-Llima, A. M. Romero, J. Menéndez, A. Rios, A. García-Sáez, and B. Juliá-Díaz, Quantum entanglement patterns in the structure of atomic nuclei within the nuclear shell model, Eur. Phys. J. A **59**, 240 (2023).

[60] R. Aoude, E. Madge, F. Maltoni, and L. Mantani, Probing new physics through entanglement in diboson production, J. High Energy Phys. 12 (2023) 017.
[61] K. Beck and G. Jacobo, Comment on "Spin correlations in elastic e^+e^- scattering in QED, Eur. Phys. J. D **77**, 85 (2023).
[62] P. J. Ehlers, Entanglement between valence and sea quarks in hadrons of $1+1$ dimensional QCD, Ann. Phys. (Amsterdam) **452**, 169290 (2023).
[63] A. Sinha and A. Zahed, Bell inequalities in 2-2 scattering, Phys. Rev. D **108**, 025015 (2023).
[64] W. K. Wootters, Entanglement of formation of an arbitrary state of two qubits, Phys. Rev. Lett. **80**, 2245 (1998).
[65] M. E. Peskin and D. V. Schroeder, *An Introduction to Quantum Field Theory* (Addison-Wesley, Reading, MA, 1995).